Available online at www.sciencedirect.com
ScienceDirect
Deep-Sea Research II 55 (2008) 277–293
DEEP-SEA RESEARCH PART II
www.elsevier.com/locate/dsr2

A first description of the Antarctic Peninsula Coastal Current

Carlos Moffat[a,*], Robert C. Beardsley[b], Breck Owens[b], Nicole van Lipzig[c]

[a]MIT/Woods Hole Oceanographic Institution Joint Program in Oceanography, Woods Hole, MA 02543, USA
[b]Physical Oceanography Department, Woods Hole Oceanographic Institution, Woods Hole, MA 02543, USA
[c]Physical and Regional Geography Research Group, Katholieke Universiteit Leuven, Belgium

Accepted 31 October 2007
Available online 27 December 2007

Abstract

We present hydrographic and shipboard ADCP data collected during the fall (April/June) and winter (July/August) and moored velocity observations collected from 2001 to early 2002 on the west Antarctic Peninsula (wAP) shelf during the Southern Ocean Global Ecosystems Dynamics (SO GLOBEC) program. In fall, a geostrophically balanced, buoyant current flows southward along the coast. This Antarctic Peninsula Coastal Current (APCC) forms during the ice-free season and extends from Adelaide Island to Alexander Island, although its path inside Marguerite Bay is uncertain. During the fall of 2001, the APCC had a volume transport of 0.32 ± 0.13 Sv and a freshwater transport (relative to a reference salinity of 34.4) of $126 \pm 50\,km^3\,yr^{-1}$. From early July to late October, the APCC disappears from the coast as the freshwater input from the coast diminishes and sea-ice forms on the shelf. An examination of the relative sizes of the freshwater sources suggests runoff from land and precipitation over the ocean are the primary sources for the APCC.
© 2007 Elsevier Ltd. All rights reserved.

Keywords: Polar oceanography; Coastal oceanography; Buoyant plumes

1. Introduction

The west Antarctic Peninsula (wAP) continental shelf hosts a rich biological community centered around Antarctic krill (*Euphasia superba*). The region has been hypothesized to act as a source for krill populations elsewhere in the Southern Ocean (Murphy et al., 1998; Hofmann and Klinck, 1998; Fach and Klinck, 2006), as well as to sustain a number of higher trophic levels in the peninsula's food web (Costa and Crocker, 1996; Fraser and Trivelpiece, 1996). Additionally, multiple studies of the regional climate have found that the surface air temperature of the peninsula is rising at one of the highest rates in the world and causing rapid changes in the region (Vaughan and Doake, 1996; Cook et al., 2005). Ocean dynamics of the wAP shelf are expected to play an important role in these processes, but they remain poorly understood. The Southern Ocean Global Ecosystem Dynamics (SO GLOBEC) field program, conducted between 2001 and 2003, was aimed at understanding the dominant physical and biological processes in Marguerite Bay and the adjacent wAP shelf region (Hofmann et al., 2002, 2004).

Prior to SO GLOBEC, the shelf circulation had been addressed by only a handful of studies, mostly involving observations of the hydrographic fields during austral summer. In a review paper, Hofmann and Klinck (1998) describe the circulation in the SO GLOBEC study area (Fig. 1) as a slow, cyclonic gyre composed of a northeastward branch flowing along the shelf break and a southward flow along the inner shelf. The shelf-break circulation is dominated by the large-scale Antarctic Circumpolar Current (ACC), while the nearshore southward flow was thought to be part of a shelf-scale gyre. However, two recent studies hint at the presence of an independent southward inner shelf circulation. Tracks of drifters released during the summer of 2001 and 2002 (as part of SO GLOBEC) show a southward current flowing along Adelaide Island and into Marguerite Bay, and then exiting on the south side of the Bay along Alexander Island (Beardsley et al., 2004). The SO

*Corresponding author. Tel.: +1 508 289 3589.
E-mail address: cmoffat@whoi.edu (C. Moffat).

0967-0645/$ - see front matter © 2007 Elsevier Ltd. All rights reserved.
doi:10.1016/j.dsr2.2007.10.003

GLOBEC regional surface dynamic topography for the fall (April–June) of 2001 is consistent with those results, and the low-salinity water found on the inner shelf suggests the flow is a buoyancy-forced coastal current (Klinck et al., 2004).

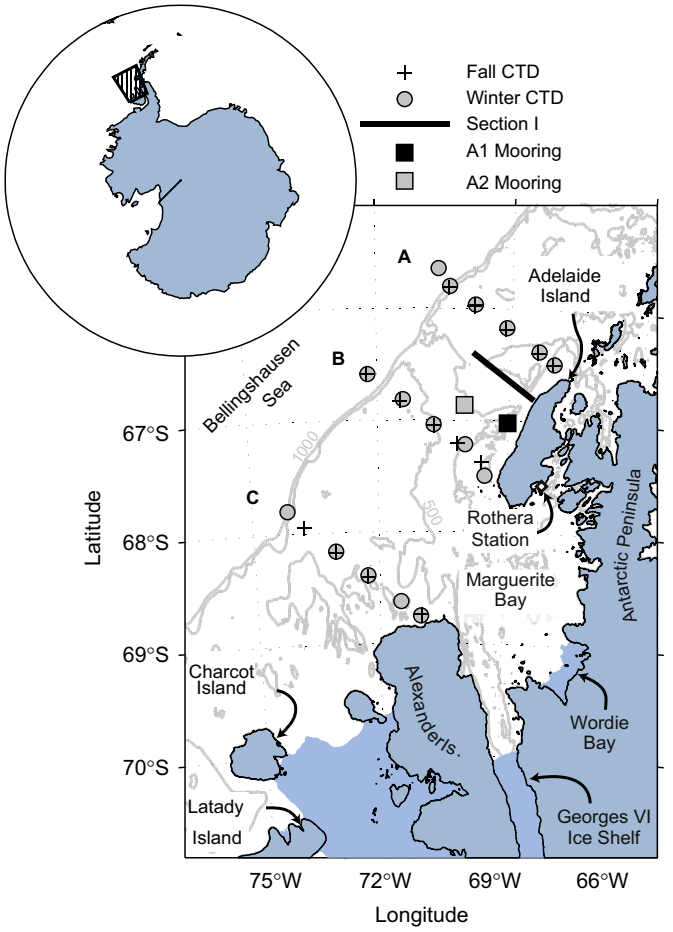

Fig. 1. The west Antarctic Peninsula (wAP) continental shelf. The gray lines indicate 500- and 1000-m isobath, and the permanent ice-shelf cover is indicated by light blue. Also shown are the A, B, and C CTD lines visited during the fall and winter survey cruises of 2001, the high-resolution Section I, the locations of the 2001 A1 and A2 Moorings and of the British Antarctic Survey Rothera Station.

Here we use the SO GLOBEC data set, including broad-scale hydrographic data and mooring observations, to provide a first description of this nearshore coastal current. We will refer to it as the Antarctic Peninsula Coastal Current (APCC). We discuss the vertical structure, transport, along-shelf variability, and seasonal evolution of the APCC. We also explore the possible forcing mechanisms and the implications of our results for the distribution of freshwater on the shelf.

2. Data sources

During 2001, two hydrographic cruises were conducted off the west coast of the Antarctic Peninsula aboard the RV/IB *N.B. Palmer* as part of the SO GLOBEC field program (Table 1). These broad-scale cruises attempted to cover the entire study region, and provided CTD (conductivity for salinity, temperature, and pressure for depth) profile observations on a grid with a nominal cross-shelf resolution of 20 km (Fig. 1). The fall survey (April 24–June 5) provided a larger spatial coverage than the winter survey (July 24–August 31), in which weather conditions and sea-ice coverage impeded navigation. Sea-surface temperature (SST) and sea-surface salinity (SSS) as well as wind speed and direction data also were collected throughout the cruises using the RV/IB *N.B. Palmer* continuous sampling systems. Details of the processing of the data set can be found in Wiebe et al. (2001) and Klinck et al. (2004).

As part of these broad-scale cruises, conductivity, temperature, and pressure data from depths of roughly 15–250 m also were collected using the Bio-Optical Multi-frequency Acoustical and Physical Environmental Recorder (BIOMAPER-II), a towed undulating multi-sensor system (Wiebe et al., 2002). A subset of these data collected on June 1, 2001 (during the fall cruise) was used to construct a high-resolution, cross-shelf hydrographic section off Adelaide Island (Fig. 1, Section I) by merging a nearshore CTD station (Station 101), the BIOMAPER data, and the underway SST and SSS data.

Velocity data were obtained during the cruises with a shipboard-mounted RD Instruments (RDI) 150-kHz narrow-band Acoustic Doppler Current Profiler (ADCP)

Table 1
Summary of the cruise dates and number of CTD stations conducted (top), and of the dates, location and local depth of the moorings deployment (bottom)

Cruise	Objective	Start	End	No. CTD Stations
LMG01-03	Mooring deployment	03/18/01	04/13/01	6
NBP01-03	Fall 2001 survey	04/24/01	06/05/01	84
NBP01-04	Winter 2001 survey	07/24/01	08/31/01	70
LMG02-1A	Mooring recovery	02/06/02	03/03/02	9

Mooring	Deployment	Recovery	Longitude	Latitude	Depth (m)
A1	03/26/01	02/13/02	69°01.217′	67°01.134′	509
A2	03/31/01	02/13/02	70°00.683′	66°51.883′	561

sampling from 31 to 431 m. The ADCP was configured with 58-m bins, an 8-m pulse length, and 5-min ensemble averages. During most of the cruise, the ADCP operated in bottom-tracking mode. The data processing was initially done during the cruise using the Common Oceanographic Data Access System (CODAS). Final processing and quality control were done by J. Hummon (University of Hawaii) and S. Howard (Earth Systems Research) (Klinck et al., 2004). ADCP data return during the winter cruise was greatly reduced while the *N.B. Palmer* was moving through sea-ice and data from those times are not considered here. For the fall cruises, the small ($<0.02\,m\,s^{-1}$) barotropic tidal currents were removed from the data set using the Antarctic Peninsula tide model, version 04.01 (AntPen04.01), a high-resolution barotropic model based on the linearized shallow water equations (L. Padman, personal communication).

Velocity, salinity, and temperature observations also were collected at the A1 mooring, located 16.3 km off the west coast of Adelaide Island at a water depth of 509 m (Fig. 2). The A1 mooring was deployed and recovered by the R/V *Laurence M. Gould* and collected data from March 2001 to February 2002 (Table 1). The mooring was equipped with SeaBird Electronics (SBE) temperature recorders at 134, 209, and 259 m depth, SBE MicroCATs measuring both temperature and salinity at 159 and 309 m, and a conductivity and temperature sensor set attached to a Vector-Averaging Current Meter (VACM) at 459 m. An SBE SeaGauge pressure sensor at 502 m recorded pressure and additional temperature and conductivity data. Velocity measurements included an upward-looking, RDI 300-kHz broadband WorkHorse ADCP located at 169 m depth and configured with 62-m bins (ranging from 47 to 165 m) and half-hour ensemble averages. Four bins (107, 109, 159, and 161 m) were replaced by linear interpolation due to contamination by the acoustic reflection from other instruments farther up on the mooring line. Finally, two VACMs also recorded currents averaged over 15-min intervals at 309 and 459 m. For details of the moored array design and data, see Moffat et al. (2005).

Ice concentration data for the study region were obtained from the Special Sensor Microwave/Imager (SSM/I) data set derived from the bootstrap passive microwave algorithm and distributed by the National Snow and Ice Data Center (NSIDC). The sea-ice data grid has a cell size of 25×25 km, and data are provided as daily averages (Comiso, 1999, updated 2005). Ice thickness data also were obtained at a series of ice stations during the winter cruise (Perovich et al., 2004), and throughout the SO GLOBEC mooring deployment (March 2001–February 2002) at the A2 mooring (Fig. 1 and Table 1), which was equipped with an Ice Profiling Sonar (IPS) deployed at the top of the mooring line. The IPS measured the acoustic range to the surface (the sea surface or ice bottom when present) every 2 s, which was then converted to distance (and thus, ice draft) using *in situ* sound speed and density calculated from a nearby sensor (Moffat et al., 2005). All

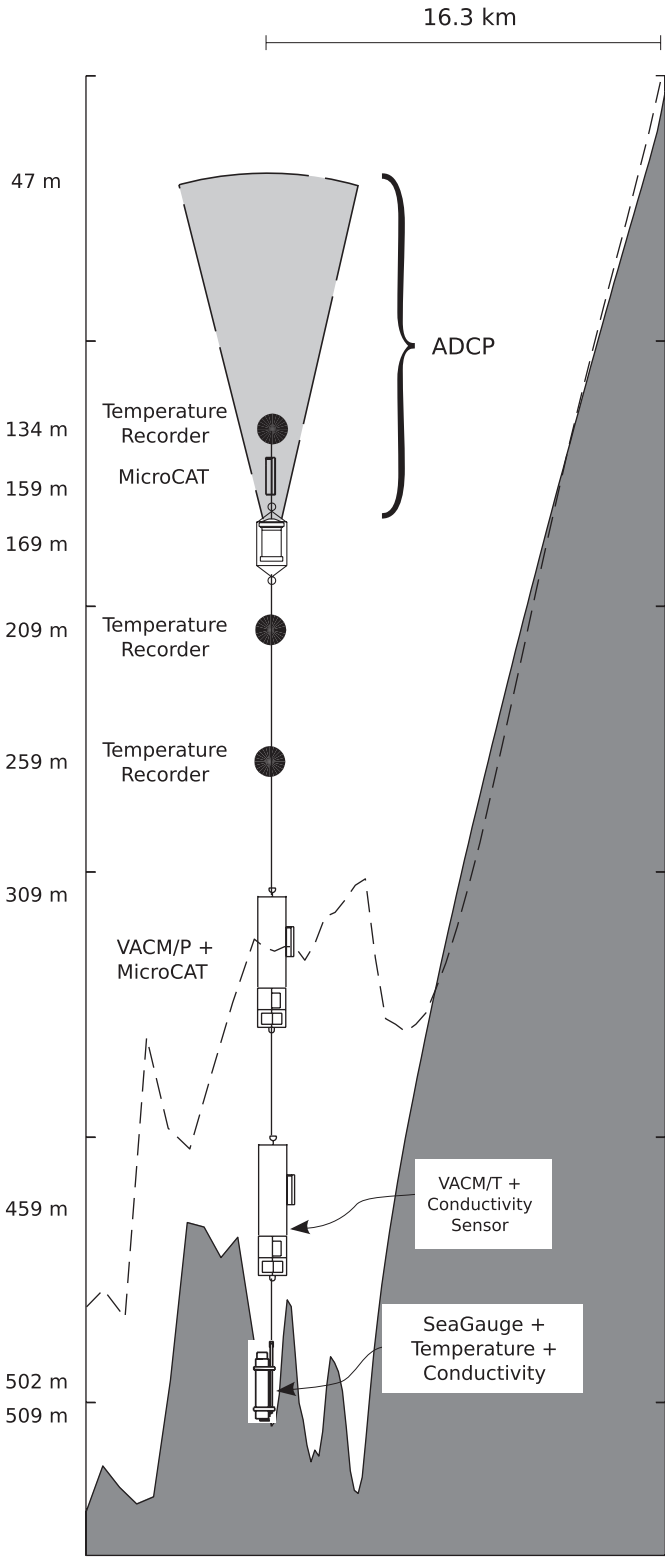

Fig. 2. Schematic of the A1 mooring, deployed during 2001 and early 2002 off Adelaide Island. One of the VACMs had a temperature recorder (VACM/T) and the other a pressure recorder (VACM/P). The dashed line shows a profile of the cross-shelf bathymetry ~3 km southwest of the mooring site.

mooring time series data shown here were low-pass filtered using a 33-h half-amplitude filter (Flagg et al., 1976; Limeburner et al., 1983) to remove tidal and inertial band

variability. All salinities are given in the practical salinity scale.

3. Background

The SO GLOBEC study area extends nearly 500 km from the northern tip of Adelaide Island to Latady Island (Fig. 1). The wAP shelf is relatively wide (≈ 130 km), deep and characterized by complex bathymetry that includes shallow plateaus and deep depressions, with mean and maximum depths of ≈400 and 1600 m, respectively (Bolmer et al., 2004). This complexity is also evident inside Marguerite Bay, where small islands, subsurface reefs, and troughs are ubiquitous.

The general features of the shelf hydrographic structure have been described in previous studies (Hofmann and Klinck, 1998; Smith et al., 1999; Klinck et al., 2004), and are illustrated by the potential temperature–salinity ($\theta-S$) diagram and vertical profiles in Fig. 3. The data were collected using a shipboard CTD at the A2 mooring site during the 2001 mooring deployment, the fall and winter cruises, and the 2002 mooring recovery (Table 1). The surface waters of the wAP region are occupied by Antarctic Surface Water (AASW), a water mass with temperatures ranging from −1.8 to 1 °C and relatively low salinities of 33.0–33.7 (Smith et al., 1999). By the end of the austral fall (end of June), strong surface heat loss leads to the formation of a deep winter mixed layer and a sea-ice cover over the entire shelf. As the sea-ice retreats and later during the ice-free season, the surface mixed layer is partially restratified by surface heating and freshening by sea-ice melt and runoff. The remnant of that cold winter mixed layer, called Winter Water (WW), is found at roughly 80- to 100-m depth during the ice-free season, with temperatures of −1 °C or less. Subpycnocline waters, below 150–200 m, are dominated by a modified version of the Circumpolar Deep Water (CDW), a warm (1.5 °C) and salty (34.6–34.73) water mass, and a source of heat and nutrients for the upper layer of the shelf (Smith et al., 1999; Serebrennikova and Fanning, 2004).

4. Structure and dynamics of the APCC

4.1. Spatial structure

During the fall cruise, maps of SSS and SST (Fig. 4) show the fresher end of the AASW near the coast, where salinities are typically lower than 33.25. These fresher waters are found along Adelaide Island and particularly in the region off Alexander Island and Charcot Island, where the surface salinity is at its minimum. SST (Fig. 4) is above zero in the northern half of the study region, and the coolest temperatures are found off Alexander and Charcot Islands, and along the shelf break. The north–south temperature gradient is likely a combination of the shelf-wide cooling during the four-week cruise, which proceeded from north to south (Klinck et al., 2004), and a mean gradient reflecting the regional climate (Stammerjohn et al., 2003).

Potential temperature-salinity ($\theta-S$) diagrams (Fig. 5) illustrate the cross-shelf hydrographic structure during the fall cruise. Far offshore, the vertical structure of the water column resembles the structure characteristic of the outer shelf and open ocean as described in Section 3 (black solid lines in Fig. 5). Near the coast, however, salinity anomalies of the order of 0.3–0.7 extend down to 100–200 m (red dashed lines in Fig. 5). Also, the subsurface temperature minimum that is the signature of the WW is much weaker near the coast than offshore. At Section C, WW is completely absent and temperature increases monotonically with depth. This absence of the WW during the fall is unique to the nearshore areas and Marguerite Bay (not shown).

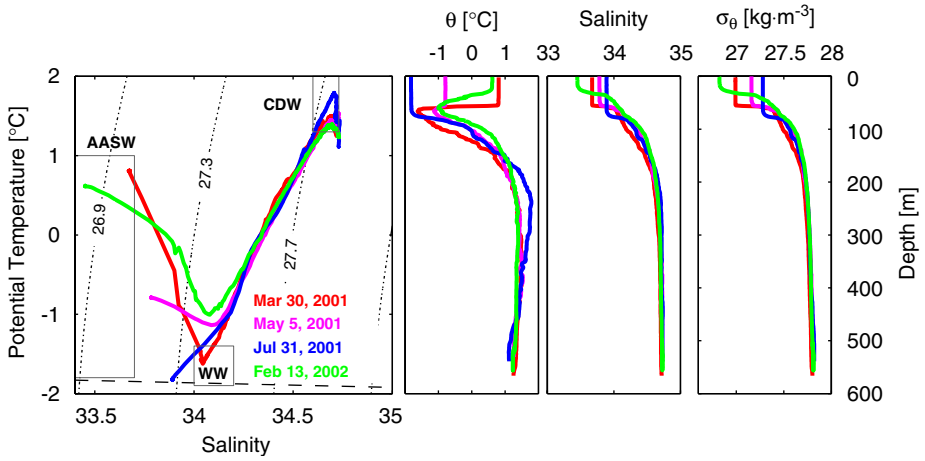

Fig. 3. Evolution of the hydrographic structure on the mid-shelf of the wAP (A2 mooring site). The left panel shows a $\theta-S$ diagram of profiles taken throughout 2001 and 2002. The gray boxes illustrate the typical range of the Antarctic Surface Water (AASW), Winter Water (WW), and Circumpolar Deep Water (CDW). The dashed line indicates the freezing point of sea-water. The right panels show the corresponding potential temperature (θ), salinity, and potential density (σ_θ) profiles.

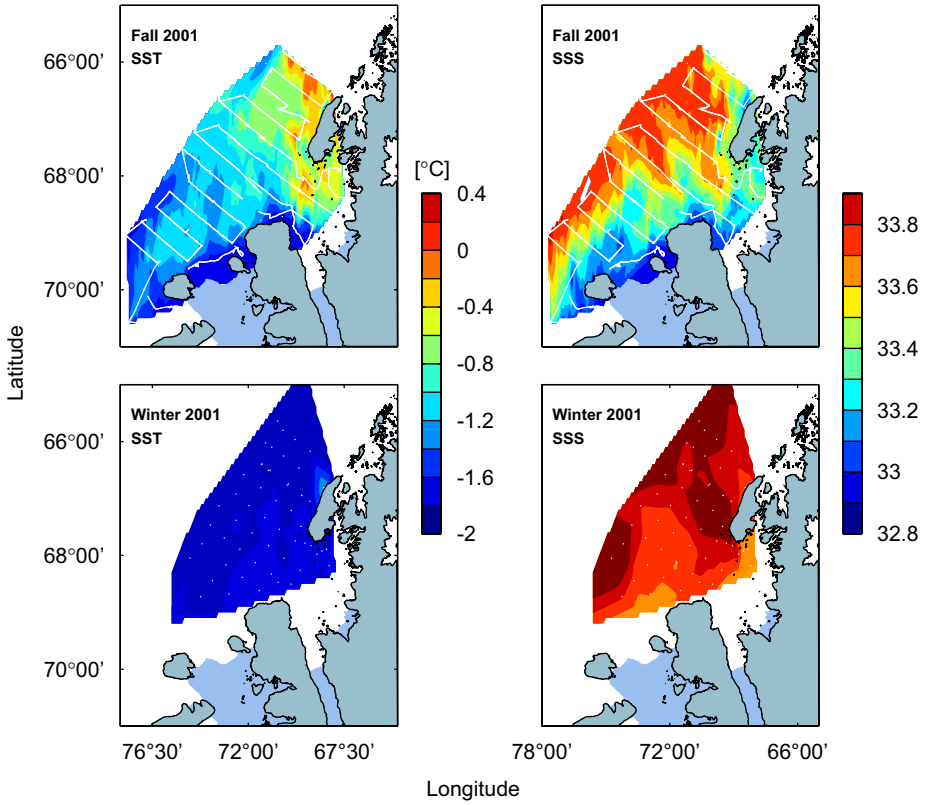

Fig. 4. Sea-surface salinity (SSS) and sea-surface temperature (SST) for the fall (CTD and underway data, top panels) and winter (CTD data, bottom panels) of 2001, collected during the SO GLOBEC broad-scale cruises on board the RV/IB *N.B. Palmer*.

A detailed hydrographic and velocity section (Fig. 6) taken off the coast of Adelaide Island (Section I, Fig. 1) shows the vertical and cross-shelf structure of the APCC. As suggested by the fall broad-scale CTD survey, freshwater is concentrated near the coast. The front separating the fresh coastal current from the shelf waters is centered 20 km off the coast. The salinity anomaly is of the order of 0.6 at the surface, and extends below 100 m and to 30 km off the coast. Unlike the shelf waters, which show a well-mixed surface layer 50–70-m deep, the surface stratification of the APCC is relatively strong, and the temperature structure differs markedly from the temperature structure of the shelf waters. WW, typically found at 80–100 m depth during the ice-free season (Fig. 3), is absent from the nearshore waters, and is replaced by a tongue of warm water out to 10 km offshore of the front. This is consistent with the absence of WW near the coast described above in the broad-scale CTD survey data (Fig. 5).

The frontal structure of the salinity field is typical of coastal buoyant plumes, and is reflected in the velocity field, which shows a well-defined coastal current co-located with the salinity front (Fig. 6). In order to obtain the velocity field above the shallowest ADCP bin (31 m, Section 2), we used the thermal wind (geostrophic) shear calculated from the hydrographic fields to extrapolate the ADCP velocity to the surface. A comparison of the mean vertical shear observed by the ADCP and the thermal wind shear averaged across the current (Fig. 7) confirms that the vertical structure of the along-shelf velocity is largely determined by the cross-shelf density gradient and validates the use of geostrophic shear to extrapolate the ADCP data vertically. Inertial motions and other wind-forced currents could strongly contaminate the characterization of the low-frequency motions we are addressing here. However, measurements from the *N.B. Palmer* indicate wind forcing was low ($<2\,\mathrm{m\,s^{-1}}$) while Section I was occupied. A wavelet analysis (not shown) of the A1 mooring velocity records showed negligible inertial frequency energy during this period.

Section I data show surface velocities approaching $0.4\,\mathrm{m\,s^{-1}}$ (Fig. 6), which decays vertically with a scale of approximately 80 m and have a horizontal scale (L) of only 5 km. The Rossby number for the current is $R_o \sim V/fL$, where f is the Coriolis parameter and V is a typical velocity. With the observed scales R_o is ≈ 0.6, an indication that nonlinear effects may be important in the along-shelf momentum balance.

Evidence of a velocity front can be found elsewhere on the shelf. Other ADCP sections off Adelaide and Alexander Islands (Fig. 8) also show nearshore flow moving with the coast to the left (Fig. 9). Although none of these sections have concurrent high-resolution hydrography that would allow examination of the dominant frontal features, freshwater fluxes and/or dynamical balances, the structure and scales observed in Sections II and III, with surface velocities of $0.15-0.40\,\mathrm{m\,s^{-1}}$ and

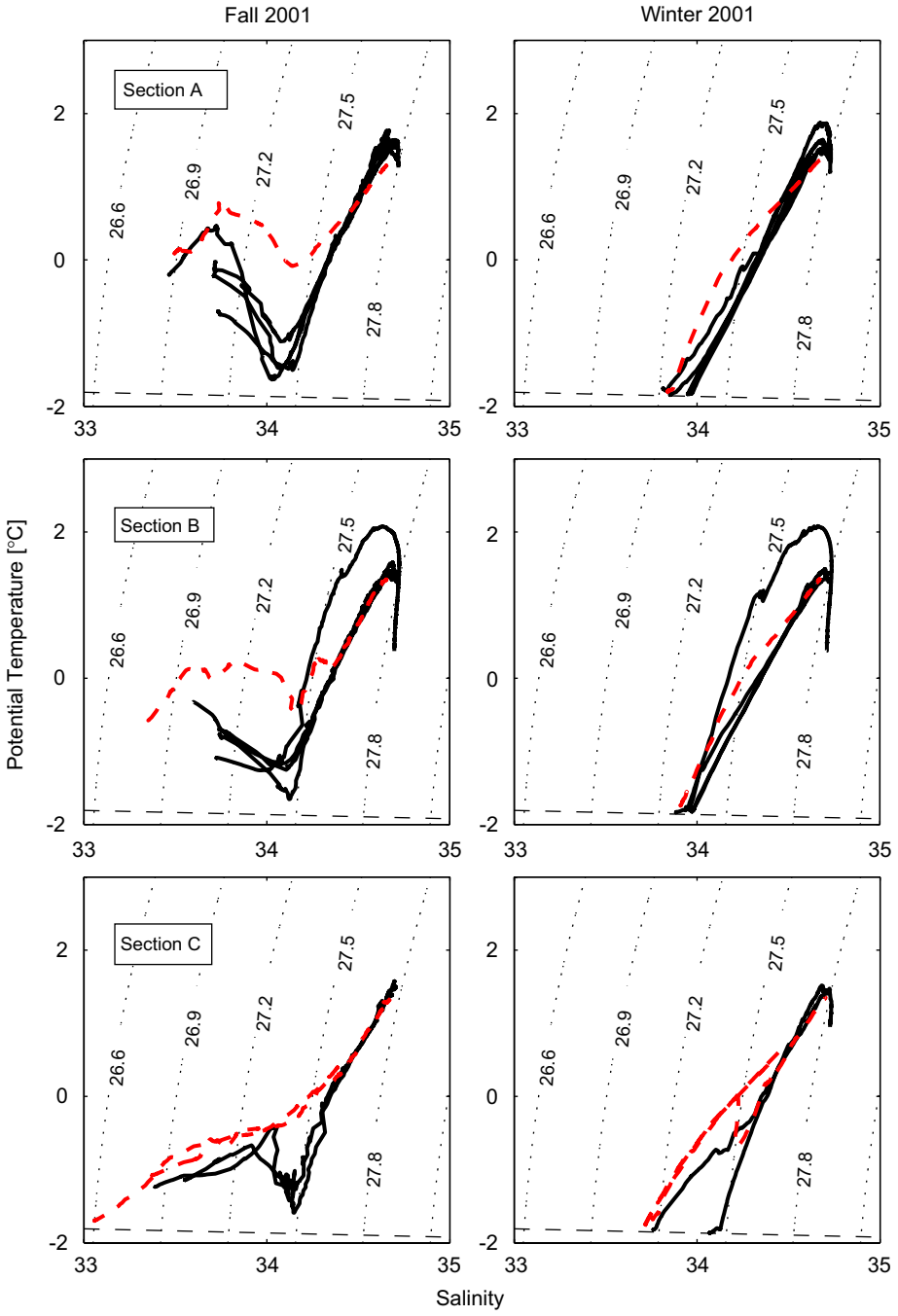

Fig. 5. Potential temperature–salinity ($\theta-S$) diagrams from line A (top panels), B (middle panels) and C (bottom panels) for the fall of 2001 (left column) and winter of 2001 (right column). The solid black lines are stations from the mid- and outer shelf, and the dashed red lines are nearshore stations. The dashed line in each panel indicates the freezing point of sea-water. Station locations are plotted in Fig. 1.

depth scales of ≈ 100 m are similar to those from Section I. Section IV is different in that the velocity front is much wider and weaker, and is also located farther offshore, a displacement perhaps forced by the shallower bathymetry of the region. Although all these observations suggest a continuous current along the shelf, it must be noted that the APCC front could not be traced within Marguerite Bay, and given the presence of other sources of freshwater within the bay, more data are required to determine the path of the APCC along the coast.

4.2. Volume and fresh water transports

The volume transport of the APCC was determined by integrating the ADCP velocity from Section I shown in Fig. 6. As a lower vertical limit for the integration, we used the 34.4 isohaline. This choice captures the frontal structure seen in the velocity field, and is also a reasonable choice for the freshwater transport. Offshore of the front, the 34.4 isohaline is typically located in the upper pycnocline, above 150 m, and is deeper than 200 m near

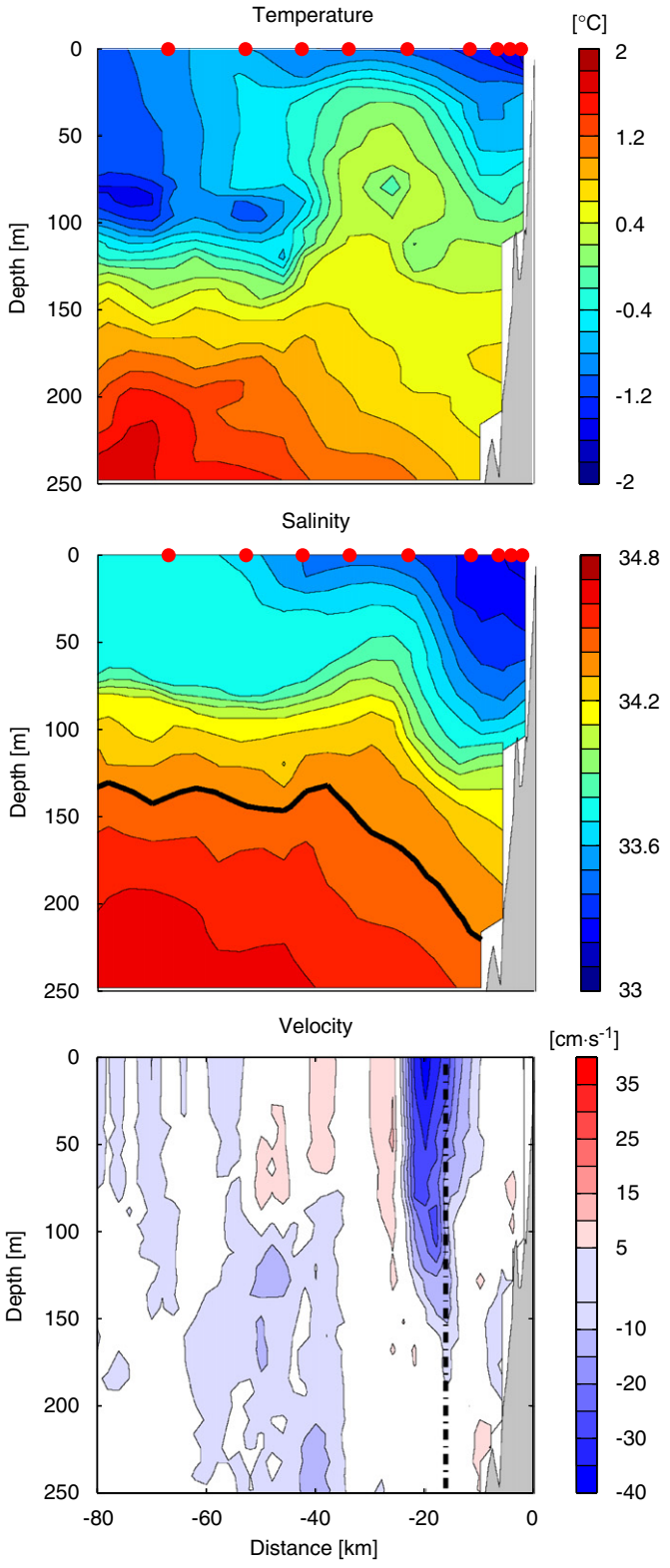

Fig. 6. Gridded temperature, salinity, and along-shelf velocity (ADCP) data from cross-shelf Section I, occupied on June 1, 2001. The red dots indicate the approximate location of BIOMAPER-II dives (top and middle panels) and the ADCP 5-min averages (bottom panel). The thick black line in the middle panel indicate the 34.4 isohaline. The dashed black line in the bottom panel indicates the approximate cross-shelf position of the A1 mooring. The along-shelf velocity is defined as the component perpendicular to the section shown in Fig. 1, with negatives values denoting flow to the southwest.

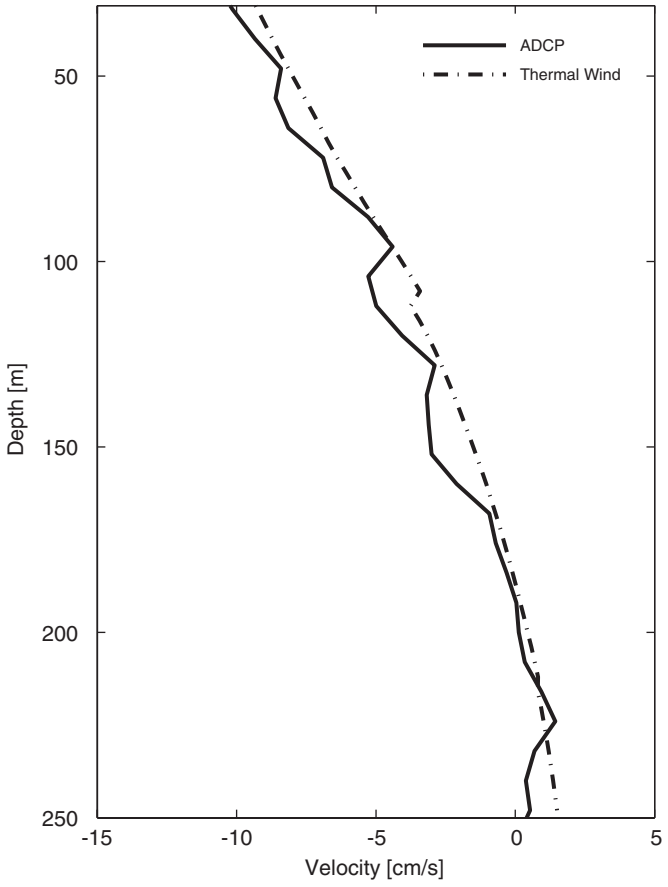

Fig. 7. Mean ADCP velocity profile for the velocity front depicted in Fig. 6 (solid) and mean velocity calculated from thermal wind shear (with an arbitrary offset) over the same cross-shelf region (4–32 km from the coast).

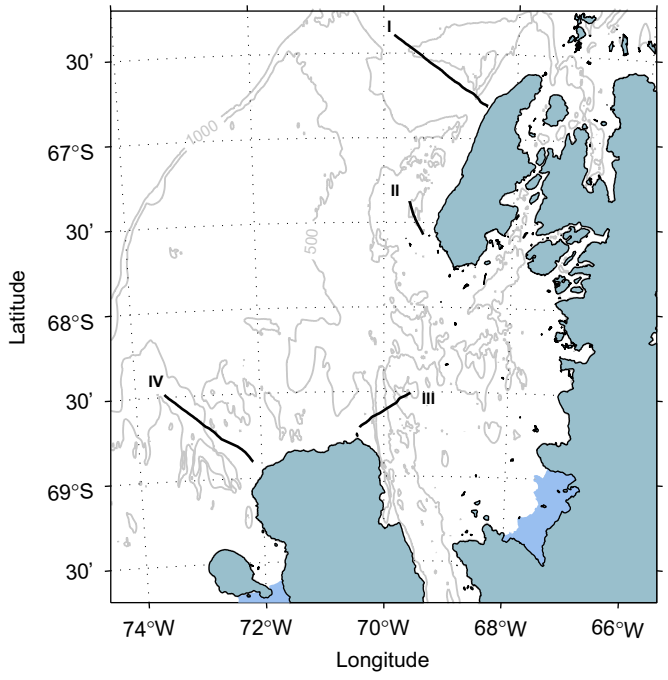

Fig. 8. Cross-shore ADCP sections collected during the fall 2001 SO GLOBEC Cruise. The lines indicate the location of Section I, and sections conducted off the southern coast of Adelaide Island (II), and off the northern (III) and western (IV) coast of Alexander Island.

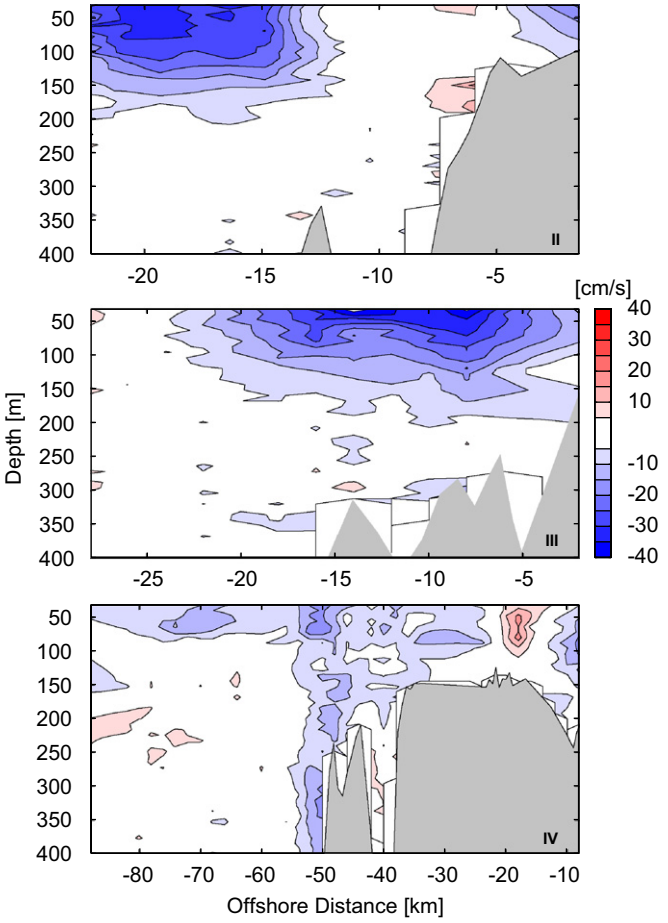

Fig. 9. Along-shelf velocity ADCP sections, with negative values indicating flow with the coast to the left. The locations of Sections II (top panel), III (middle panel), and IV (bottom panel) are shown in Fig. 8. The thin solid lines near the topography delineate the boundary for the velocity estimates.

the coast (Fig. 6). The integration from the 34.4 isohaline to the surface and from the coast offshore to 24 km results in a total transport of 0.32 ± 0.13 Sv. The associated freshwater transport of the APCC in Section I is given by

$$\mathrm{FWT} = \int_A \frac{S - S_\mathrm{r}}{S_\mathrm{r}} v \, \mathrm{d}A, \tag{1}$$

where v is the along-shelf velocity, S is the observed salinity, S_r is a reference salinity (chosen here as 34.4), and A is the total area enclosed by the isohaline and an offshore limit of 24 km. This results in a value of FWT of approximately $126 \pm 50\,\mathrm{km^3\,yr^{-1}}$ for Section I (for convenience, we take both the volume and the freshwater transports as positive quantities). This value is obtained by assuming the APCC is present on the shelf for seven months of the year. The work presented in the discussion section provides the basis for this assumption.

The uncertainty in the two transport estimates (about 40%) can be explained as follows. Systematic instrumental errors have been removed during post-processing of the data (see Section 2 and references therein), and other instrumental errors are assumed to be negligible when the data are integrated over the entire section. Tidal currents are small (as discussed before) and have been removed using a regional tidal model. The A1 mooring data provide a good estimate of the synoptic variability of the APCC during the fall season. This variability might be due to temporal variability in the transport, as well as cross-shelf displacements of the front of the APCC. An estimate of both effects can be calculated from the ratio of the mean velocity to the standard deviation of the fall along-shelf velocity, which is of the order of 35%. As we are unable to separate temporal variability from horizontal displacements of the front, we assume all of this uncertainty is due to temporal variability. An additional source of uncertainty is the vertical extrapolation of the ADCP data using the thermal wind shear. Apart from this calculation, we attempted two other methods of extrapolation: linear extrapolation and assuming a constant velocity from the shallowest ADCP bin to the surface. The resulting spread added an additional 5% or so of uncertainty to the transport calculation, giving a total uncertainty of about 40%.

4.3. Comparison with theoretical scales

Several studies have explored the processes and dynamics that determine the relevant scales of a geostrophically balanced coastal buoyant plume (Yankovsky and Chapman, 1997; Fong and Geyer, 2001; Lentz and Helfrich, 2002). Using the data from Section I, we can compare some simple theoretical scalings to those observed in the APCC. Among those scales are the along-shelf volume transport (Q), the total width of the current (W_p), and the width of the front (W_s). Assuming a buoyant plume in geostrophic balance over a motionless deep layer, the volume transport as a function of the distance offshore can be estimated from

$$Q(x) = \frac{g'}{2f}(h_p^2 - h(x)^2), \tag{2}$$

where g' is the reduced gravity $g\Delta\rho/\rho$, $\Delta\rho$ is the density difference between the plume and the ambient water, g is the gravitational acceleration, h_p is the depth at which the front touches the bottom, and h is the depth of the front at a distance x offshore of the foot of the front. In this model, all of the transport Q is associated with the front, and the region onshore of the foot of the front is motionless. If the isopycnal chosen to characterize the front outcrops and the integration is carried out over the entire region enclosed by that isopycnal, h becomes zero and the volume transport Q becomes independent of x. The width of the front scales with the internal radius of deformation ($W_s = \sqrt{g'h_p}/f$), and the total width of the current is then $W_p = W_s + W_b$, where W_b is the horizontal distance from shore to the isobath h_p (Fig. 10; modified from Lentz and Helfrich, 2002).

Using the same 34.4 isohaline used in the previous section provides a meaningful comparison with the observed

along-shelf transport, as the velocity below the chosen isohaline is reasonably close to zero (a basic assumption in the derivation of Eq. (2)). This isohaline touches the bottom at $h_p = 220$ m, and the depth h at the offshore limit of the front is ≈ 170 m. The reduced gravity is computed using the observed density difference across the density front. Using either the density difference at the surface or the average density difference above the 34.4 isohaline results in $\Delta\rho \sim 0.45$ and $g' \approx 4.3 \times 10^{-3}\,\mathrm{m\,s^{-2}}$. Using $f = 1.34 \times 10^{-4}\,\mathrm{s^{-1}}$, the theoretical volume transport Q is ≈ 0.31 Sv and the front width W_s is ≈ 7 km.

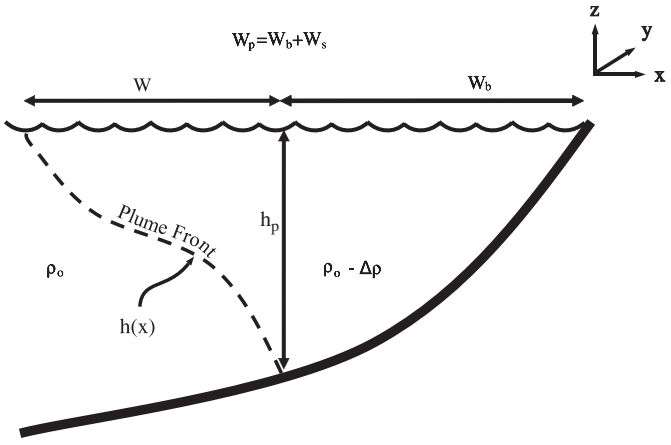

Fig. 10. Schematic of the relevant scales of a coastal buoyant plume. The plume front, of width W_s, separates the shelf water of density ρ_o from the lighter (by $\Delta\rho$) nearshore water. The front depth is h and the front touches the bottom at h_p and a distance from the coast W_b (modified from Lentz and Largier, 2006).

The width of the front is estimated from the observations as the decay scale of the along-shelf velocity maximum on the surface layer, and is approximately 5 ± 2 km. Both the width and the volume transport calculated from the data in Section I are in good agreement with the theoretical scales (0.31 Sv and 7 km, respectively), suggesting that the observed current is a coastal plume in geostrophic balance to lowest order. However, the observations show the total width (W_p) of the APCC is larger than expected from the model sketched in Fig. 10. In the model, the buoyant plume adjusts to a final state where the near-bottom velocity is zero and the front can be found attached to depth h_p. Our observations suggest that the front is farther offshore than expected, so that the total width is greater than $W_b + W_s$. This can also be observed in the hydrographic data, which show nearly flat isopleths in the upper 120 m or so of the water column onshore of 10 km. This is a possible result of the APCC adjusting to some upstream bathymetric feature or local forcing, or the violation of some of the assumptions of the simple theoretical model used here.

4.4. Temporal evolution: the winter shutdown

As the winter approaches, heat loss from the ocean to the atmosphere increases significantly, eventually leading to the formation of sea-ice on the shelf. As a result, SST during the winter months (Fig. 4) is nearly at the freezing point everywhere. SSS is also strongly modified, showing higher values (partially explained by brine rejection), and dramatically reduced horizontal gradients compared to those for the fall.

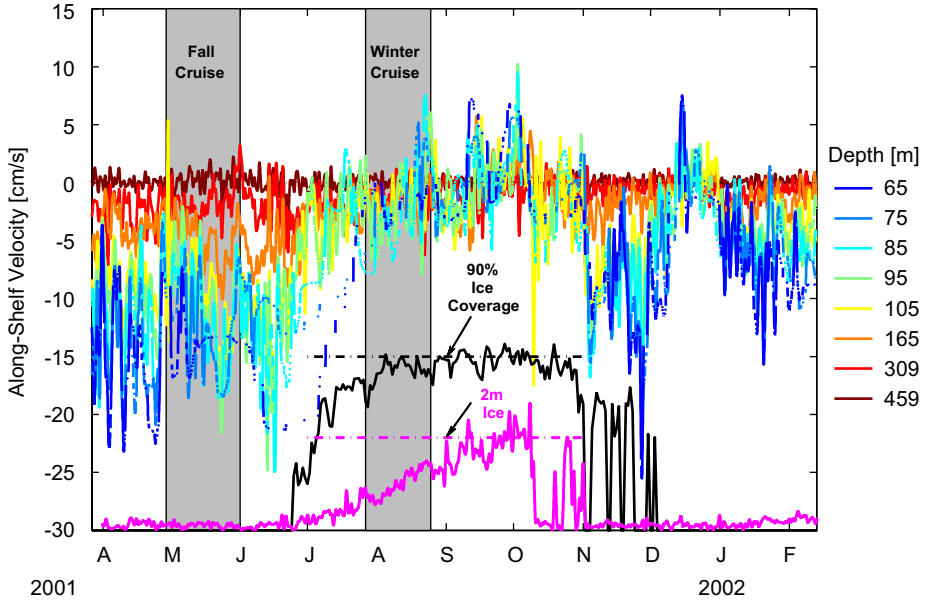

Fig. 11. Time series of along-shelf (positive northeastwards) velocity at the A1 mooring (68° 01.217′W, 67° 01.134′S). The colored lines show velocity at different depths from the upward-looking ADCP (65–165 m) and VACMs (309 and 459 m). The shaded areas indicate periods when the fall and winter broad-scale cruises were conducted. The black line shows the sea-ice concentration (in percent) for the nearest grid point to the A1 mooring site from the Special Sensor Microwave/Imager (SSM/I) Satellite data (Comiso, 1999). The magenta line shows the sea-ice draft (in meters) measured with the IPS at the A2 mooring.

Due to the sea-ice and harsh weather conditions, no high-resolution shipboard ADCP or BIOMAPER-II survey data were collected during the 2001 winter cruise. However, the surface fields (Fig. 4) suggest the horizontal density gradients are greatly diminished when the shelf is ice covered. This is confirmed by the winter CTD θ/S diagrams (Fig. 5, right-hand panels), which show reduced horizontal gradients of properties during the winter cruise when the surface layers have become colder and saltier. Although a freshwater anomaly can still be found near the coast in winter, it is much smaller than that found during the fall cruise.

Despite the lack of detailed cross-shelf sections of hydrography or velocity during winter, the A1 mooring, deployed 16.3 km offshore of Adelaide Island (Fig. 1), was favorably located to explore how the changing hydrographic structure and sea-ice conditions affect the evolution of the coastal current throughout the year. Low-pass filtered ADCP and VACM velocities from the A1 mooring, sampling the water column from 65 to 459 m, are plotted in Fig. 11. During the fall, the mooring data reflect the strongly baroclinic structure evident in the hydrographic and velocity sections off Adelaide Island (Section 4.1). Velocities in the shallowest depth bin (65 m) are typically 0.15 to 0.20 m s^{-1}, and deep velocities remain small throughout the year. The A1 site mooring was located in a deep depression with a downstream (in the sense of the APCC flow) sill depth of around 320 m (the mooring depth is 509 m—Fig. 2), which might explain the small near-bottom velocities observed. These near-bottom velocities are not unlike others found elsewhere on the shelf in the SO GLOBEC study area where sills and deep depressions are ubiquitous (Moffat et al., 2005).

The SSM/I satellite ice concentration time series clearly show the rapid onset and slow retreat of ice cover typical of the wAP region (Fig. 11; Stammerjohn et al., 2003). As the shelf transitions from ice-free to mostly ice covered at the beginning of July 2001, the along-shelf current is abruptly reduced (Fig. 11). The ice-draft time series from the A2 mooring is consistent with the satellite data and also shows gradual growth in thickness of the sea-ice cover, reaching a draft of 2 m by mid-September. By the time the 2001 winter cruise was conducted, there is little sign of a coherent along-shelf flow at A1, suggesting that the APCC has completely shut down. Velocities during the ice-covered period rarely exceed 0.05 m s^{-1}, and northeastward flow ($v<0$), virtually non-existent during the fall, is frequent during the winter.

This evolution is also evident in the seasonally averaged mooring records (Fig. 12), which show a strong along-shelf velocity profile during the fall (defined here until June, before the onset of the sea-ice on early July), with velocities in the shallower bins of 0.20 m s^{-1} or more and a depth scale exceeding 100 m. The winter profile shows significant variability in the top 90 m, but the seasonal mean is small throughout most of the water column. After the sea-ice retreats from the region in early November, a significant

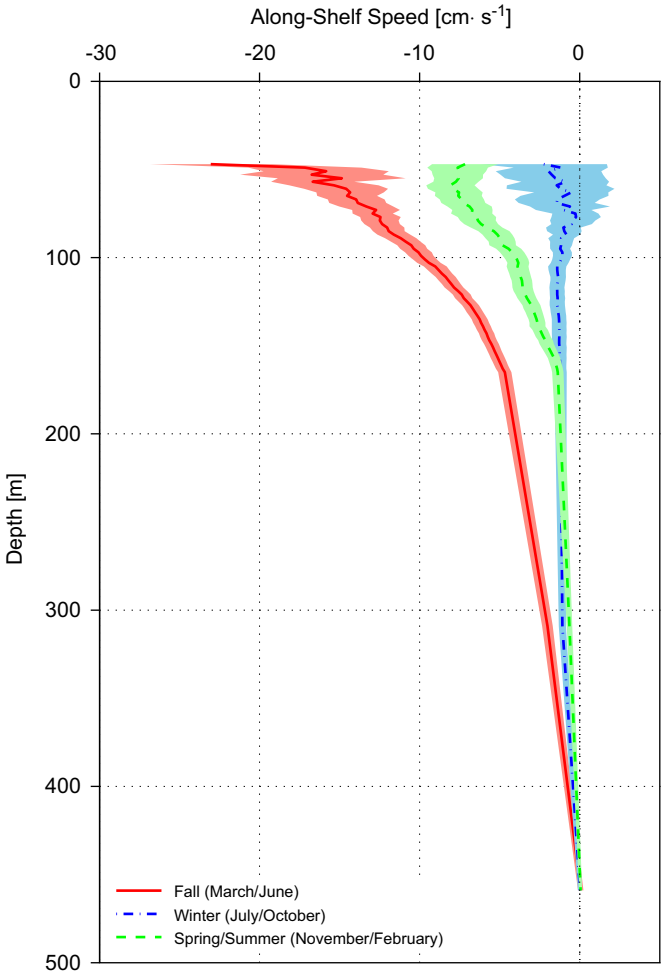

Fig. 12. Average of along-shelf velocities from the A1 mooring records for the fall (February–June), winter (here defined as the ice-covered season, from July to October) and spring/summer (from November to the end of the deployment, in February) shown in Fig. 11. The lines indicate the mean values for the season, and the shading the standard error.

along-shelf flow reappears with a smaller seasonal mean, reflecting the reduction of the velocity and brief flow reversal in mid-December. Although the seasonal change may be due to cross-shelf displacements of the front, the broad-scale CTD surveys during the winter (discussed above) show significant reduction of the cross-shelf density gradients, consistent with the shutdown of the coastal current. Ice breakup and retreat starts in mid- to late-October 2001 and is evident in the satellite ice concentration data as well as in the A2 ice-draft time series. As the sea-ice retreats, a coherent southward along-shelf flow reappears, and is only interrupted in mid- to late-December, when a strong reduction of the along-shelf velocity was observed.

5. Discussion

The freshwater sources which force the APCC are difficult to quantify due to the lack of reliable, continuous observations of freshwater inputs to the shelf. We will

attempt to enumerate and quantify these sources and discuss their relative importance in the context of a freshwater budget for a coastal region upstream of Section I. We finish with a brief discussion of the effects of wind forcing on the APCC.

5.1. Fresh water budget

Unlike buoyant plumes formed by riverine outflow (e.g., Yankovsky and Chapman, 1997; Whitney and Garvine, 2005; Lentz and Largier, 2006), where most of the freshwater can be traced back to a single upstream source, the inputs for the APCC are multiple and are distributed along the coast. A freshwater budget for the APCC upstream of Section I can be written as

$$\mathrm{FWT} = U + \langle R\rangle + \langle P-E\rangle_{\mathrm{ocean}} + \langle M_{\mathrm{ice}}\rangle + \langle O\rangle, \tag{3}$$

where FWT is the freshwater transport measured at Section I and U is the freshwater transport at some point upstream of Section I. The other terms refer to the influx of freshwater between that upstream point and Section I: R is the runoff from land, $P-E_{\mathrm{ocean}}$ is the precipitation minus evaporation that occurs over the ocean, and M_{ice} is the sea-ice melt. Other sources or sinks of freshwater, such as cross-shelf Ekman transport, eddies, etc. are represented by O and are not considered further, as we have no information about them. Integration of the terms over a given region upstream of Section I is represented by brackets ($\langle\,\rangle$). Because there are no simultaneous observations of the terms on the right-hand side of the freshwater budget above, we assume instead that FWT from Section I is a reasonable estimation of the climatological freshwater transport of the APCC, and use both published data and results from an atmospheric regional model to estimate the right-hand side terms of Eq. (3).

5.1.1. Evidence for the APCC upstream of Section I

A brief review of the available literature on the circulation north of Section I can shed light on the approximate size of the upstream region influencing the nearshore freshwater budget at Section I, and the size of U. Near the tip of the Antarctic Peninsula, the Antarctic Coastal Current (Fahrbach et al., 1992) has been observed to flow northwards and to continue counter-clockwise around the tip and then westwards into the Bransfield Strait (Heywood et al., 2004). Carrying water with T/S properties similar to those of the APCC, the Antarctic Coastal Current was found to transport ≈ 1 Sv into Bransfield Strait, although its path after it entered the strait could not be determined (Heywood et al., 2004).

Studies of the surface circulation in the Bransfield and Gerlache Straits, using drifter observations and hydrographic data, suggest the dominant feature in this region is flow crossing from the northern section of Gerlache Strait to the southern coast of the South Shetland Islands, although meanders and recirculations are common elsewhere in this area (Niiler et al., 1990; Huntley and Niiler, 1995; Zhou et al., 2002). This northward circulation from Gerlache Strait to Bransfield Strait suggests that the path of the Antarctic Coastal Current might retroflect within this region rather than continue along the shelf and toward the SO GLOBEC study region. This is consistent with summertime observations from the Palmer Long Term Ecological Research (LTER) program, which show minimal amounts of mixing between Bransfield Strait waters and the waters farther south (Capella et al., 1992; Smith et al., 1999).

For the region south of Bransfield Strait, a few published observations show a southward circulation between Anvers Island and Section I. A drifter released in Gerlache Strait on December 1991 moved to the southwest along the coast (Huntley and Niiler, 1995), and another drifter passing by Anvers Island also moved to the southwest in the last few months of 1979 (Hofmann et al., 1996). This is consistent with LTER observations, which showed the presence of a cross-shelf density gradient and geostrophic flow to the southwest near the coast south of Anvers Island (Smith et al., 1999). In summary, there is little observational evidence of a continuous southward circulation from Bransfield Strait to the shelf south of Anvers Island, suggesting that the APCC has a relatively local origin somewhere between Anvers Island and Section I. Thus, we take U to be zero and consider the freshwater budget

$$\mathrm{FWT} = \langle R\rangle + \langle P-E\rangle_{\mathrm{ocean}} + \langle M_{\mathrm{ice}}\rangle \tag{4}$$

for the region from Anvers Island to Section I (Fig. 13).

5.1.2. Runoff from land

The mass budget of the land ice on the Antarctic Peninsula is given by

$$\frac{\mathrm{d}M}{\mathrm{d}t} = \langle P-E\rangle_{\mathrm{land}} - \langle R\rangle - \langle C\rangle, \tag{5}$$

where M is the mass of the land ice, $\langle P-E\rangle_{\mathrm{land}}$ is the precipitation minus evaporation over the land ice, R is the net runoff, and C represents iceberg calving into the ocean. Although there is no quantitative information about the size of C, icebergs that melt locally are a net input of freshwater to the nearshore ocean. Lacking better information, we assume $R \gg C$ (or equivalently, we assume icebergs melt primarily near the coast), and we estimate the runoff from land as

$$\langle R\rangle = \langle P-E\rangle_{\mathrm{land}} - \frac{\mathrm{d}M}{\mathrm{d}t}. \tag{6}$$

Thus, net runoff from land is understood here to represent the net precipitation minus evaporation over land ($\langle P-E\rangle_{\mathrm{land}}$) minus long-term land-ice change $\mathrm{d}M/\mathrm{d}t$. Note that downstream of Section I, the George VI ice shelf is expected to make a significant contribution to the budget, as studies suggest there are 53 km yr^{-1} of basal melt for the entire ice shelf (Potter and Paren, 1985), and therefore the runoff term would include such contribution.

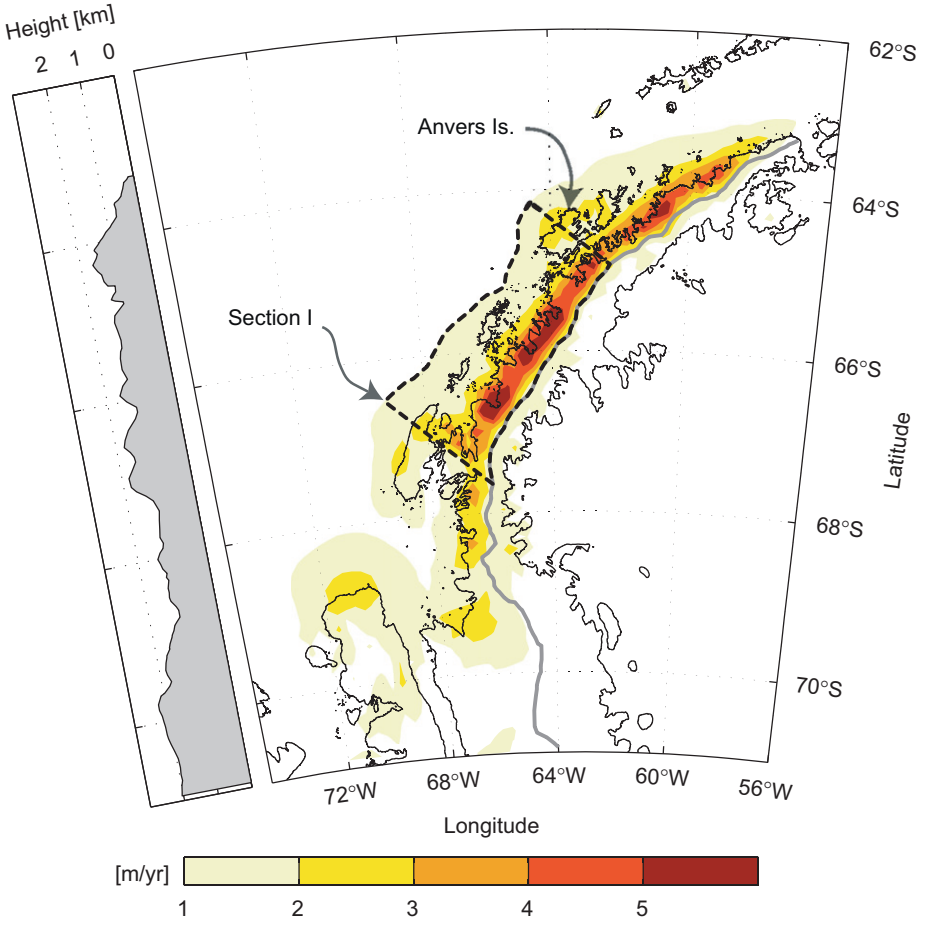

Fig. 13. Modeled precipitation minus evaporation ($P-E$) map for the wAP region (data from van Lipzig et al., 2004). The thick gray line indicates the location of the spine of the peninsula (from the RACMO14 topography), and the height of the topography along the spine is plotted on the left panel. The dashed black line indicates the region upstream of Section I used to compute the freshwater budget.

Both the mountainous topography of the peninsula and a consistently westerly atmospheric flow contribute to the wAP having the largest precipitation rate in Antarctica (van Lipzig et al., 2004). Since *in situ* measurements are sparse, van Lipzig et al. (2004) used a regional atmospheric mesoscale model to quantify the spatial variability in surface precipitation minus evaporation ($P-E$). This Regional Atmospheric Climate MOdel (RACMO14), using a horizontal grid spacing of 14 km, was integrated for the period 1987–1993. The annually averaged model output (Fig. 13) shows $P-E$ values in excess of $2\,\mathrm{m\,yr^{-1}}$ along most of the west drainage basin of the peninsula north of Marguerite Bay. In the SO GLOBEC study region, high values are found along the west coast of Adelaide Island, the northeast coast of Marguerite Bay, Wordie Bay, and the northern coast of Alexander Island.

In order to calculate the annually averaged input of freshwater to the ocean from the land $\langle P-E\rangle_{\mathrm{land}}$, we need to define the eastern boundary of the region between Anvers Island and Section I where the integration will be carried out. We used the RACMO14 topography to find the spine of the peninsula, i.e. the limit of the western drainage basin (Fig. 13). The integration of the 7-yr average $P-E$ over the land, integrated from Anvers Island to Section I and from the spine of the peninsula to the coast, results in an influx of $68\pm20\,\mathrm{km^3\,yr^{-1}}$ (±1 standard deviation). Here, we assume the freshwater accumulated over land during the winter is discharged to the ocean preferentially during the ice-free season, as is suggested by the results of Meredith et al. (2008). The uncertainty above includes only 1 standard deviation of the monthly averaged model output, and not the differences with observations or other sources of error.

The Antarctic Peninsula is one of the fastest-warming regions in the world, with mean surface atmospheric warming of $2.5-3\,^{\circ}\mathrm{C}$ since 1951, accompanied by a $1\,^{\circ}\mathrm{C}$ warming of the ocean's surface (King, 1994; Vaughan and Doake, 1996; Meredith and King, 2005). Of the 244 glaciers draining the Antarctic Peninsula ice sheet, 87% have retreated in the period between 1940 and 2004, and retreat rates are accelerating (Cook et al., 2005). Although few published estimates exist of the secular freshwater flux resulting from this process, an extrapolation of the retreat rates of glaciers melting into Wordie Bay (a small bay within Marguerite Bay, Fig. 1) to a region including the west basin of the peninsula from its tip to Wordie Bay

suggests $20 \pm 6\,km^3$ of freshwater may be lost to the ocean every year (Rignot et al., 2005). A separate study estimated the runoff as a result of the increasing number of melting days on the peninsula to be between 2.9 and $20\,km^3\,yr^{-1}$ (for comparison purposes, we convert this range to an average of $11.5 \pm 8.5\,km^3 yr^{-1}$). This estimate included the entire peninsula (including west and east drainage basins) for the year 2000 (Vaughan, 2006). Assuming the same rates for the $\approx 19200\,km^2$ region used in our budget, and averaging the estimates of the two studies cited, we obtain a dM/dt of $-6 \pm 4\,km^3\,yr^{-1}$. Adding the estimate of $\langle P-E\rangle_{land}$ north of Section I and the size of dM/dt discussed above, our estimate for $\langle R\rangle$ is therefore $74 \pm 20\,km^3\,yr^{-1}$.

5.1.3. Precipitation minus evaporation over the ocean

Uplift of air occurs upstream of the mountains of the Antarctic Peninsula, resulting in high precipitation rates over the nearshore ocean of the wAP (van Lipzig et al., 2004), as illustrated in Fig. 13. Cross-shelf profiles of $P-E$ upstream of Section I suggests this input decays from the coast with an offshore scale of $\approx 25\,km$. In order to quantify the importance of this component, the $P-E$ field over the ocean is integrated from Anvers Island to Section I and from the coast offshore to the $1\,m\,yr^{-1}$ $P-E$ isopleth (some 20–50 km off the coast). This results in $27 \pm 7\,km^3\,yr^{-1}$ of freshwater input to the nearshore ocean from $\langle P-E\rangle_{ocean}$. This integration only includes the influx during the seven ice-free months of the year (from November to June), and not during the winter months (July–October), consistent with Section 5.1.4 (see below) and the freshwater transport calculation at Section I.

5.1.4. Sea-ice melt

Sea-ice is formed at the end of the fall and throughout the winter, creating a seasonal cover that slowly retreats during the spring (Stammerjohn et al., 2003). Sea-ice samples collected during the 2001 SO GLOBEC winter cruise had an average thickness of $62 \pm 44\,cm$ (Perovich et al., 2004). Relative to other places in the Southern Ocean, the wAP shelf region has high precipitation rates and relatively thin sea-ice (Perovich et al., 2004; van Lipzig et al., 2004). This leads to proportionally deep snow and negative sea-ice freeboard, setting the conditions for significant surface flooding, refreezing, and snow-ice formation.

Quantifying the contribution of sea-ice melt M_{ice} to the freshwater budget of the APCC is particularly difficult. Ice formed from sea-water and melted in the same location does not generate, over a yearly cycle, a net input of freshwater. Other dynamics, however, are potentially important. Below, we discuss two mechanisms to input freshwater near the coast related to sea-ice: shoreward sea-ice drift and precipitation near the shore stored throughout the winter as snow and snow-ice.

Evidence for sea-ice drift has been reported in several regional studies of sea-ice dynamics. The meridional atmospheric circulation plays an important role in determining the extent and composition of the sea-ice cover, by both advecting the existing sea-ice and opening and closing leads where sea-ice production is enhanced (Stammerjohn et al., 2003; Massom et al., 2006; Harangozo, 2006). In nearshore areas, wind forcing can result in a significant amount of compaction and rafting of the sea-ice. This process was especially dramatic during the 2001–2002 season, when anomalously strong northwesterly winds were reported to cause rafting of sea-ice near the shore, reaching a thickness of 10–15 m during an October cruise in mid-Marguerite Bay (Massom et al., 2006).

High snowfall rates, another source of freshwater input, are also evident in the SO GLOBEC sea-ice measurements. A mass balance buoy was deployed on August 6, 2001, on sea-ice initially 0.65 m thick with 0.25 m of snow on top. The buoy functioned through November 10, mostly within 100 km or so from the northern shore of Alexander Island and measured an increase of snow thickness of approximately 1 m (Perovich et al., 2004, Fig. 10). Although the accumulation for the rest of the year is unknown and the density of the snow cover was not recorded, these rates of snowfall are an indication that the rates of $1-2.5\,m\,yr^{-1}$ of water equivalent suggested by the atmospheric model's climatology for approximately the same region are reasonable (Fig. 13). Using the same region as in Section 5.1.3, the model output results in $37 \pm 12\,km^3\,yr^{-1}$ of mean freshwater accumulation over the winter months (July–October).

As the sea-ice retreats and melts throughout the spring (and into summer), the freshwater input from both shoreward advection of ice and precipitation will contribute to the observed APCC freshwater transport. The resulting meltwater will presumably leave the region of interest. An estimate of the timescale for this signal to propagate alongshore away from the region can be obtained by estimating the propagation speed of a buoyant plume of finite along-shelf length trapped against the coast. In the absence of any other forcing, the leading and trailing edges (the "nose") of the plume will propagate at a speed given by

$$c_p \sim \frac{c_w}{1 + W_b/W_w}, \tag{7}$$

where c_p is the nose speed of the plume and $c_w = (2g'Qf)^{1/4}$ is the nose speed of a plume if it were moving along a vertical wall (Lentz and Helfrich, 2002). The ratio W_b/W_w (Fig. 10) describes the importance of a bottom slope in the dynamics, with surface-trapped plumes having ratios closer to zero. Using W_b/W_w from 0.1 to 10 and the observed transport and density anomaly from Section I, Eq. (7) gives c_p of $\sim 0.7 - \sim 0.07\,m\,s^{-1}$, respectively. With this scaling, which assumes the density anomaly generated by sea-ice melting would be as large as the observed one, the freshwater signal would propagate through the ~270-km long stretch from Anvers Island to Adelaide Island in five days to six weeks. Even at the slowest estimate, it would

seem that sea-ice, which decays to a minimum extent during the summer (Stammerjohn et al., 2003), would have a maximum impact on the freshwater budget considered here during the spring and early summer, and not during the fall, when the data discussed here were taken.

A few other data sets address the relevance of sea-ice to the nearshore freshwater budget. Hydrographic data taken off Anvers Island from 1991 to 1999 suggest the summer nearshore freshwater is largely explained by runoff detected as pulses of freshwater in nearshore stations throughout the summer, and not melted sea-ice (Dierssen et al., 2002). Also, $\delta^{18}O$ measurements collected close to the British Antarctic Survey Rothera Station in Marguerite Bay during 2002 and 2003 were used to quantify the relative contributions of sea-ice and freshwater runoff from land to the local upper-column freshwater content. These observations suggest runoff from land is largely responsible for the freshwater found in the surface layer, and that this runoff has a significant seasonal signal, with maximum input from February to June (Meredith et al., 2008). However, it must be noted that the oxygen isotope samples were collected on the leeward side of Adelaide Island, so snow and snow-ice accumulation over the sea ice is not expected to be as large as on the windward side, where Section I is located (Fig. 13).

In summary, we expect sea-ice melt to play a potentially important role in the freshwater budget of the APCC, in particular as the sea-ice melts during the spring and the $37 \pm 12\,km^3\,yr^{-1}$ that the model output suggest have accumulated on the ice start melting. The details of how this freshwater is discharged to the ocean and quantification of the sea-ice drift contribution are difficult to determine at this point, but sea-ice is likely not relevant to the discussion of the freshwater budget when using observations taken in June. At the end of the fall, we expect most of the sea-ice to have melted and the associated freshwater anomaly to have propagated away from the region considered here. We therefore assume this component to be zero, with the important caveat that our reasoning here must be tested using new field measurements and high-resolution models of this region.

5.1.5. Total freshwater input upstream of Section I

The sum of runoff from land ($\langle P-E\rangle_{land}$ and $\langle dM/dt\rangle$) and precipitation over the ocean ($\langle P-E\rangle_{ocean}$) could contribute $101 \pm 22\,km^3\,yr^{-1}$ of freshwater to the coastal ocean from Anvers Island to Section I (Eq. (3)), with an unknown contribution from sea-ice and other sources and sinks. Given our estimates of the freshwater upstream of Section I ($126 \pm 50\,km^3\,yr^{-1}$—Section 4.2), this suggests $\langle R\rangle$ and $\langle P-E\rangle_{ocean}$ are the primary sources of freshwater for the APCC. In the previous section, we argued that sea-ice is of secondary importance to the forcing of the APCC during summer and fall. The freshwater budget is certainly affected by sea-ice formation and melting, although near the coast, it is the runoff from land that appears to play a dominant role (Meredith et al., 2008). In this scenario, the driving factor is the reduction of air temperature as winter arrives. This causes both sea-ice formation and reduction of freshwater input from the land, but it is the latter that would be responsible for the shutdown of the APCC (Section 4.4). However, our estimation of the transport (based on a single shipboard ADCP section), the sources for our estimation of the freshwater influx, and our knowledge of the local sea-ice distribution and dynamics are subject to significant uncertainty, so additional observations are necessary to better determine the relative contributions of the different freshwater sources to the forcing of the APCC.

5.2. Wind effects

While on June 1, 2001 when the data in Section I were collected, the winds were rather weak ($<2\,m\,s^{-1}$), strong downwelling-favorable winds are prevalent in this region near the coast. They are expected to significantly affect the structure and dynamics of the APCC. Although the response of coastal buoyant currents to downwelling-favorable winds is not well understood, it is known that it will force a cross-shelf Ekman transport near the surface and an additional along-shelf, geostrophically balanced flow that can increase the observed transport of the current (Fong and Geyer, 2001; Whitney and Garvine, 2005; Lentz and Largier, 2006).

Assuming a simple model with linear bottom stress balancing the wind stress, the wind-driven along-shelf transport is $Q_w = \tau/(\rho_o r)A$, where τ is the along-shelf wind stress, ρ is a reference density, A is the cross-sectional area of the plume and, r is a bottom drag coefficient, taken here as $5 \times 10^{-4}\,m\,s^{-1}$ (Lentz and Largier, 2006). Wind measurements collected in Marguerite Bay (Moffat et al., 2005) from June 2001 to April 2003 have a mean along-shelf wind stress of $-0.04 \pm 0.14\,N\,m^{-2}$ (± 1 standard deviation), and a maximum value of $-1.71\,N\,m^{-2}$ (here, the coordinate system is the same used for Section I, so negative values indicate downwelling-favorable winds). Over the same area enclosed by the 34.4 isohaline and a 24-km offshore limit, which resulted in a volume transport of 0.32 Sv (Section 4.1), Q_w is 0.28 Sv for the mean wind stress (note we compare the transports for the same area, but the region onshore of the front would likely not be motionless when subjected to wind forcing). Although this model is very simple, it illustrates the sensitivity of our transport calculations to wind forcing, and highlights the importance of concurrent atmospheric measurements on the wAP shelf when considering the dynamics of the APCC.

6. Summary and open questions

Observations collected during 2001–2002 as part of the Southern Ocean GLOBEC program reveal the presence of a buoyancy-forced, geostrophically balanced coastal current along the west coast of the Antarctic Peninsula, from Adelaide Island to Alexander Island. The Antarctic

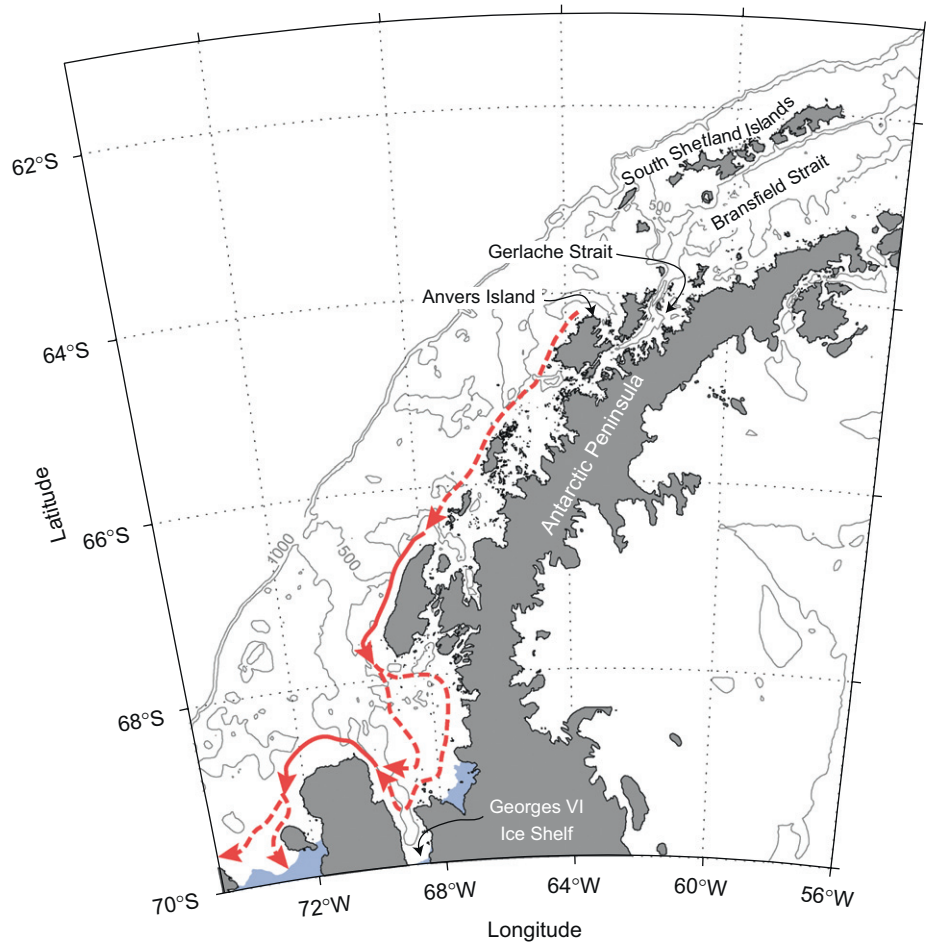

Fig. 14. Schematic of the path of the APCC. The solid lines indicate sections along the coast where the velocity front and a cross-shelf density gradient was observed. The dashed lines are suggested paths, not derived from observations.

Peninsula Coastal Current (APCC) is strongly seasonal and forms during the spring/summer when the shelf is ice-free. The APCC is characterized by a surface density anomaly of $\sim 0.6\,\mathrm{kg\,m^{-3}}$ and surface velocities of the order of $0.30-0.40\,\mathrm{m\,s^{-1}}$. One high-resolution hydrographic and velocity section off the coast of Adelaide Island suggests the volume transport of the APCC is of order $0.32 \pm 0.13\,\mathrm{Sv}$ with a freshwater transport of order $126 \pm 50\,\mathrm{km^3\,yr^{-1}}$. Three additional ADCP sections along the coast show a velocity front consistent with a coastal buoyant current off Adelaide and Alexander Islands (Fig. 14).

Moored observations show the virtual disappearance of the APCC during the winter months, after sea-ice forms on the shelf and the melt-water fluxes from the coast are drastically reduced. As the sea-ice breaks up and melts with increasing insolation and air temperature, the APCC reappears. Output from a regional atmospheric model and a review of the literature suggest runoff from land and precipitation over the ocean, when integrated from Anvers Island south, can provide roughly enough freshwater to the nearshore ocean to explain the observed freshwater transport of the APCC off Adelaide Island. Other sources and sinks, like ice-melt, wind-driven Ekman transport, and eddies were not considered, but may play an important role. Previous studies reviewed here suggest the wAP region presents particularly favorable conditions (high $P-E$, retreating glaciers, downwelling-favorable winds) for the formation of a coherent seasonal coastal buoyant current.

Many questions remain. Although it is likely that the continuous freshwater influx along the peninsula makes the APCC a ubiquitous feature along the coast of the wAP south of Anvers Island, more detailed observations are required to determine its path in the SO GLOBEC study region. Of particular interest is the path (or paths) of the APCC inside Marguerite Bay, which could not be determined with our data set.

An important point that needs to be investigated is the interannual variability of the APCC. Researchers have found significant interannual variability in upper-ocean characteristics (Dierssen et al., 2002; Meredith et al., 2004) and sea-ice (Stammerjohn et al., 2003; Perovich et al., 2004; Harangozo, 2006) among others, and much of that variability is likely to directly impact the APCC. Observations designed to monitor its strength and along-shelf

variability seem necessary to gauge the overall importance of the APCC on the wAP system.

Also, we have not addressed the connections of the APCC to the rich biological communities present on the wAP. Several recent studies of the biological communities in this region have observed strong cross-shelf gradients in biogeochemical variables. Chlorophyll (Dierssen et al., 2002), nutrient deficits (Serebrennikova and Fanning, 2004), and plankton concentrations (Ashjian et al., 2004; Lawson et al., 2004; Lawson et al., 2008) are high along the coast. This suggests that the APCC might be key to providing a favorable environment for biological production. This might be due to a variety of reasons: a coastal buoyant current like the APCC retains freshwater and nutrients (like trace metals) contained therein near the shore, it has relatively high stratification, and could be host to a biological community well adapted to the cold and low-salinity water maintained by the current. Also, the APCC provides a path for the along-shelf transport of biogeochemical tracers and plankton during the ice-free season. This advection is likely to be an important factor to explain biomass and nutrient fluxes in and out of Marguerite Bay. The ongoing synthesis effort of the SO GLOBEC data sets and further research into these and other questions should help address some of the many issues raised here.

Acknowledgments

We want to thank the crew of the research vessels L.M. Gould and N.B. Palmer for their help in the collection of the data used here. We also want to thank Richard Limeburner (WHOI) and Scott Worrilow (WHOI) and his crew in the Subsurface Mooring Operations Group and the Rigging Shop at WHOI for the successful deployment and recovery of the moored array and the preliminary data processing. Jason Hyatt helped obtain and process the SSM/I and ice draft data, and provided helpful discussions of ice dynamics on the wAP shelf. John Klinck (Old Dominion University) provided the hydrographic data. Peter Wiebe, Carin Ashjian, and Gareth Lawson (all at WHOI) provided the BIOMAPER-II data for Section I. We are indebted to Mike Meredith (British Antarctic Survey) and coauthors for sending us a manuscript of their oxygen isotope work, which provided valuable insight into the freshwater budget in Marguerite Bay. Melanie Fewings, Tom Farrar, Dave Sutherland, and Steve Lentz (all at WHOI), as well as Mike Meredith and an anonymous reviewer provided valuable comments to improve this manuscript. This work was supported by the National Science Foundation Office of Polar programs through US Southern Ocean GLOBEC grants OPP 99-10092 and ANT 05-23223. The atmospheric modelling was performed at the British Antarctic Survey (BAS) with funding from a European Commission Marie Curie Fellowship for Nicole van Lipzig and high-performance computer facilities provided by the Computer Services for Academic Research (CSAR). C. Moffat also received support from the Chilean government through its Presidential Fellowship program and the Coastal Ocean Institute at WHOI and the Cooperative Institute for Climate and Ocean Research at WHOI. This is US GLOBEC contribution number 538.

References

Ashjian, C., Rosenwaks, G., Wiebe, P., Davis, C., Gallager, S., Copley, N., Lawson, G., Alatalo, P., 2004. Distribution of zooplankton on the continental shelf off Marguerite Bay, Antarctic Peninsula, during Austral fall and winter, 2001. Deep-Sea Research II 51 (17–19), 2073–2098.

Beardsley, R.C., Limeburner, R., Owens, W.B., 2004. Drifter measurements of surface currents near Marguerite Bay on the western Antarctic Peninsula shelf during austral summer and fall, 2001 and 2002. Deep-Sea Research II 51 (17–19), 1947–1964.

Bolmer, S., Beardsley, R., Pudsey, C., Morris, P., Wiebe, P., Hofmann, E., Anderson, J., Maldonado, A., 2004. A High-Resolution Bathymetry Map for the Marguerite Bay and Adjacent Western Antarctic Peninsula Shelf for the Southern Ocean GLOBEC Program. Technical Report WHOI-2004-02, Woods Hole Oceanographic Institution.

Capella, J., Ross, R., Quetin, L., Hofmann, E., 1992. A note on the thermal structure of the upper ocean in the Bransfield Strait-South Shetland Islands region. Deep-Sea Research-Oceanographic Research Papers 39 (7–8), 1221–1229.

Comiso, J., 1999, updated 2005. Bootstrap Sea Ice concentrations for NIMBUS-7 SMMR and DMSP SSM/I, January 2001 to March 2002. Boulder, CO, USA, digital Media.

Cook, A.J., Fox, A.J., Vaughan, D.G., Ferrigno, J.G., 2005. Retreating glacier fronts on the Antarctic Peninsula over the past half-century. Science 308, 541–544.

Costa, D., Crocker, D., 1996. Marine mammals of the Southern Ocean. In: Ross, R., Hofmann, E., Quetin, L., (Eds.). Foundations for Ecological Research West of the Antarctic Peninsula, of Antarctic Research Series vol. 70, American Geophysical Union, pp. 287–301.

Dierssen, H.M., Smith, R.C., Vernet, M., 2002. Glacial meltwater dynamics in coastal waters west of the Antarctic Peninsula. Proceedings of the National Academy of Sciences 99 (4), 1790–1795.

Fach, B., Klinck, J., 2006. Transport of Antarctic krill (Euphausia superba) across the Scotia Sea. Part I: circulation and particle tracking simulations. Deep-Sea Research I 53 (6), 987–1010.

Fahrbach, E., Rohardt, G., Krause, G., 1992. The Antarctic Coastal Current in the southeastern Weddell Sea. Polar Biology 12 (2), 171–182.

Flagg, C.N., Vermersch, J.A., Beardsley, R.C., 1976. 1974 MIT New England shelf dynamics experiment (1974) data report, Part II: the moored array. Technical Report 76-1, Massachusetts Institute of Technology.

Fong, D., Geyer, W.R., 2001. Response of a river plume during an upwelling favorable wind event. Journal of Geophysical Research 106 (C1), 1067–1084.

Fraser, W., Trivelpiece, W., 1996. Factors controlling the distribution of seabirds: winter–summer heterogeneity in the distribution of Adélie penguin populations. In: Ross, R., Hofmann, E., Quetin, L., (Eds.) Foundations for ecological research west of the Antarctic Peninsula, of Antarctic Research Series vol. 70, American Geophysical Union, pp. 257–272.

Harangozo, S., 2006. Atmospheric circulation impacts on winter maximum sea ice extent in the west Antarctic Peninsula region (1979–2001). Geophysical Research Letters 33 (2), L02502.

Heywood, K., Garabato, A., Stevens, D., Muench, R., 2004. On the fate of the Antarctic Slope Front and the origin of the Weddell Front. Journal of Geophysical Research 109, C06021.

Hofmann, E., Klinck, J., 1998. Hydrography and circulation of the antarctic continental shelf 150°E to the Greenwich Meridian. In:

Robinson, A., Brink, K. (Eds.), The Sea, vol. 11. Wiley Sons, New York, pp. 997–1042 (Chapter 35).

Hofmann, E., Klinck, J., Lascara, C., Smith, D., 1996. Water mass distribution and circulation west of the Antarctic Peninsula and including Bransfield Strait. In: Ross, R., Hofmann, E., Langdon, B. (Eds.), Foundations for Ecological Research West of the Antarctic Peninsula, of Antarctic Research Series, vol. 70, American Geophysical Union, pp. 61–80.

Hofmann, E., Klinck, J., Costa, D., Daly, K.L., Torres, J., Fraser, W., 2002. U.S. Southern Ocean Global Ocean Ecosystem Dynamics Program. Oceanography 15(2), 64–74.

Hofmann, E.E., Wiebe, P., Costa, D.P., Torres, J.J., 2004. An overview of the Southern Ocean Global Ocean Ecosystems Dynamics program. Deep Sea Research II 51 (17–19), 1921–1924.

Huntley, M.E., Niiler, P.P., 1995. Physical control of population dynamics in the Southern Ocean. ICES Journal of Marine Science 52, 457–468.

King, J.C., 1994. Recent climate variability in the vicinity of the Antarctic Peninsula. International Journal of Climatology 14 (4), 357–369.

Klinck, J.M., Hofmann, E.E., Beardsley, R.C., Salihoglu, B., Howard, S., 2004. Water-mass properties and circulation on the west Antarctic Peninsula continental shelf in austral Fall and Winter 2001. Deep-Sea Research II 51 (17–19), 1925–1946.

Lawson, G., Wiebe, P., Ashjian, C., Gallager, S., Davis, C., Warren, J., 2004. Acoustically-inferred zooplankton distribution in relation to hydrography west of the Antarctic Peninsula. Deep-Sea Research II 51 (17–19) 2041–2072.

Lawson, G.L., Wiebe, P.H., Ashjian, C.J., Stanton, T.K., 2008. Euphausiid distribution along the Western Antarctic Peninsula—(B) distribution of euphausiid aggregations and biomass, and associations with environmental features. Deep-Sea Research II, this issue [doi:10.1016/j.dsr2.2007.11.014].

Lentz, S., Helfrich, K., 2002. Buoyant gravity currents along a sloping bottom in a rotating fluid. Journal of Fluid Mechanics 464, 251–278.

Lentz, S.J., Largier, J., 2006. The influence of wind forcing on the Chesapeake Bay buoyant coastal current. Journal of Physical Oceanography 36 (7), 1305–1316.

Limeburner, R., Alessi, C.A., Beardsley, R.C., Rosenfeld, L.K., Lentz, S.J., Send, U., Winant, C.D., Allen, J.S., Halliwell Jr., G.R., Brown, W.S., Irish, J.D., 1983. CODE-2: moored array and large-scale data report. Technical Report 85-35, Woods Hole Oceanographic Institution.

Massom, R., Stammerjohn, S., Smith, R., Pook, M., Iannuzzi, R., Adams, N., Martinson, D., Vernet, M., Fraser, W., Quetin, L., Ross, R.M., Massom, Y., Krouse, H.R., 2006. Extreme anomalous atmospheric circulation in the west Antarctic Peninsula region in austral spring and summer 2001/02, and its profound impact on sea ice and biota. Journal of Climate 19 (15), 3544–3571.

Meredith, M., Renfrew, I., Clarke, A., King, J., Brandon, M., 2004. Impact of the 1997/98 ENSO on upper ocean characteristics in Marguerite Bay, western Antarctic Peninsula. Journal of Geophysical Research 109, C09013.

Meredith, M.P., Brandon, M.A., Wallace, M.I., Clarke, A., Leng, M.J., Renfrew, I.A., van Lipzig, N., King, J.C., 2008. Variability in the freshwater balance of northern Marguerite Bay, Antarctic Peninsula: results from δ^{18}O. Deep-Sea Research II, this issue [doi:10.1016/j.dsr2.2007.11.005].

Meredith, M.P., King, J.C., 2005. Rapid climate change in the ocean west of the Antarctic Peninsula during the second half of the 20th century. Geophysical Research Letters 32 (L19604).

Moffat, C., Beardsley, R., Limeburner, R., Owens, W., Caruso, M., Hyatt, J., 2005. Southern Ocean GLOBEC moored array and automated weather station data report. Technical Report WHOI-2005-07, Woods Hole Oceanographic Institution.

Murphy, E., Watkins, J., Reid, K., Trathan, P., Everson, I., Croxall, J., Priddle, J., Brandon, M., Brierley, A., Hofmann, E., 1998. Interannual variability of the South Georgia marine ecosystem: biological and physical sources of variation in the abundance of krill. Fisheries Oceanography 7 (3–4), 381–390.

Niiler, P., Illeman, J., Hu, J., 1990. RACER: Lagrangian drifter observations of surface circulation in the Gerlache and Bransfield Straits. Antarctic Journal of the United States 25, 134–137.

Perovich, D.K., Elder, B.C., Claffey, K.J., Stammerjohn, S., Smith, R., Ackley, S.F., Krouse, H.R., Gow, A.J., 2004. Winter sea-ice properties in Marguerite Bay, Antarctica. Deep-Sea Research II 51 (17–19), 2023–2039.

Potter, J., Paren, J., 1985. Interaction between ice shelf and ocean in George VI Sound, Antarctica. In: Jacobs, S. (Ed.), Oceanology of the Antarctic Continental Shelf, Antarctic Research Series, vol. 43, American Geophysical Union, pp. 35–58.

Rignot, E., Casassa, G., Gogineni, S., Kanagaratnam, P., Krabill, W., Prichard, H., Rivera, A., Thomas, R., Turner, J., Vaughan, D., 2005. Recent ice loss from the Fleming and other glaciers, Wordie Bay, West Antarctic Peninsula. Geophysical Research Letters 32 (L07502).

Serebrennikova, Y.M., Fanning, K.A., 2004. Nutrients in the Southern Ocean GLOBEC region: variations, water, circulation and cycling. Deep-Sea Research II 51 (17–19), 1981–2002.

Smith, D.A., Hofmann, E., Klinck, J., Lascara, C., 1999. Hydrography and circulation of the west Antarctic Peninsula continental shelf. Deep-Sea Research I 46, 925–949.

Stammerjohn, S.E., Drinkwater, M.R., Smith, R.C., Liu, X., 2003. Ice–atmosphere interactions during sea-ice advance and retreat in the western Antarctica Peninsula region. Journal of Geophysical Research 108 (C10), 3329.

van Lipzig, N.P.M., King, J.C., Lachlan-Cope, T.A., van den Broeke, M.R., 2004. Precipitation, sublimation, and snow drift in the Antarctic Peninsula region from a regional atmospheric model. Journal of Geophysical Research 109, D24109.

Vaughan, D., Doake, C., 1996. Recent atmospheric warming and retreat of ice shelves on the Antarctic Peninsula. Nature 379 (6563), 328–331.

Vaughan, D.G., 2006. Recent trends in melting conditions on the Antarctic Peninsula and their implications for ice-sheet mass balance and sea level. Arctic, Antarctic, and Alpine Research 38 (1), 147–152.

Whitney, M., Garvine, R., 2005. Wind influence on a costal buoyant overflow. Journal of Geophysical Research 110, C03014.

Wiebe, P., Hofmann, E., Beardsley, R.C., Ribic, C., Chapman, E., Ashjian, C., Gallager, S., Davis, C., Koz-lowski, W., Friedlaender, A., Berchok, C., Rutherford, C., Warren, J., Fisher, K., 2001. Report of RV/IB Nathaniel B. Palmer cruise 01-03 to the western Antarctic Peninsula 24 April to 5 June 2001. United States Southern Ocean Global Ocean Ecosystems Dynamics program. Technical Report Number 2.

Wiebe, P., Stanton, T., Greene, C., Benfield, M., Sosik, H., Austin, T., Warren, J., Hammar, T., 2002. BIOMAPPER-II: an integrated instrument platform for coupled biological and physical measurements in coastal and oceanic regimes. IEEE Journal of Oceanic Engineering 27 (3), 700–716.

Yankovsky, A., Chapman, D., 1997. A simple theory for the fate of buoyant coastal discharges. Journal of Physical Oceanography 27, 1386–1400.

Zhou, M., Niiler, P., Hu, J., 2002. Surface currents in the Bransfield and Gerlache Straits, Antarctica. Deep-Sea Research I 49 (2), 267–280.